

Inmunoglobulin light chain enhancer hijacking activates *CCND2* and *CCND3* in cyclin D1-negative mantle cell lymphoma

David Martín-García^{*1,2}, Alba Navarro^{*1,2}, Rafael Valdés-Mas³, Guillem Clot^{1,2}, Jesús Gutiérrez-Abril³, Miriam Prieto^{1,2}, Inmaculada Ribera-Cortada⁴, Renata Woroniecka⁵, Grzegorz Rymkiewicz⁶, Susanne Bens^{7,8}, Laurence de Leval⁹, Andreas Rosenwald¹⁰, Judith A. Ferry¹¹, Eric D. Hsi¹², Kai Fu¹³, Jan Delabie¹⁴, Dennis Weisenburger¹⁵, Daphne de Jong¹⁶, Fina Climent¹⁷, Sheila J. O'Connor¹⁸, Steven H. Swerdlow¹⁹, David Torrents^{20,21}, Sergi Beltran²², Blanca Espinet²³, Blanca González-Farré^{2,24}, Luis Veloza²⁴, Dolors Costa^{2,24}, Estela Matutes²⁴, Reiner Siebert^{7,8}, German Ott²⁵, Leticia Quintanilla-Martinez²⁶, Elaine S. Jaffe²⁷, Carlos López-Otín^{2,3}, Itziar Salaverria^{1,2}, Xose S. Puente^{2,3#}, Elias Campo^{1,2,23,28#}, Sílvia Bea^{1,2#}

¹Institut d'Investigacions Biomèdiques August Pi i Sunyer (IDIBAPS), Barcelona, Spain

²Centro de Investigación Biomédica en Red de Cáncer (CIBERONC), Madrid, Spain

³Departamento de Bioquímica y Biología Molecular, Instituto Universitario de Oncología, Universidad de Oviedo, Oviedo, Spain

⁴Hospital Nostra Senyora de Meritxell, Escaldes-Engordany, Principat d'Andorra

⁵Cytogenetic Laboratory and ⁶Department of Pathology and Laboratory Diagnostics, Maria Sklodowska-Curie Institute - Oncology Center, Warsaw, Poland

⁷Institute of Human Genetics, Ulm University and Ulm University Medical Center, Ulm, Germany

⁸Institute of Human Genetics, Christian-Albrechts-University Kiel and University Hospital Schleswig-Holstein, Campus Kil, Kiel Germany

⁹Institut de Pathologie, Centre Hospitalier Universitaire Vaudois, Lausanne, Switzerland

¹⁰Institute of Pathology, University of Würzburg, and Comprehensive Cancer Center Mainfranken, Würzburg, Germany

¹¹Department of Pathology, Massachusetts General Hospital, and Harvard Medical School, Boston, Massachusetts, USA

¹²Cleveland Clinic Foundation, Cleveland, OH, USA

¹³Departments of Pathology and Microbiology and Hematology Oncology, University of Nebraska Medical Center, Omaha, NE, USA

¹⁴University of Toronto and Oslo University Hospital, Oslo, Norway

¹⁵Department of Pathology, City of Hope National Medical Center, Duarte, CA, USA

¹⁶VU University Medical Center, Amsterdam, The Netherlands

¹⁷Hospital Universitari de Bellvitge-IDIBELL, L'Hospitalet de Llobregat, Spain

¹⁸HMDS Laboratory, Leeds Teaching Hospitals NHS Trust, St James's Institute of Oncology, Leeds, UK

¹⁹Department of Pathology, University of Pittsburgh School of Medicine, Pittsburgh, PA, USA

²⁰Joint BSC-CRG-IRB Research Program in Computational Biology, Barcelona Supercomputing Center, Barcelona, Spain

²¹Institució Catalana de Recerca i Estudis Avançats (ICREA), Barcelona, Spain.

²²Centre Nacional d'Anàlisi Genòmica (CNAG)-Centre for Genomic Regulation (CRG), Barcelona, Spain

²³Laboratori de Citogenètica Molecular, Servei de Patologia, Hospital del Mar, Barcelona, Spain; Grup de Recerca Translacional en Neoplàsies Hematològiques, Cancer Research Programme, IMIM-Hospital del Mar, Barcelona, Spain

²⁴Hematopathology Section, Hospital Clínic de Barcelona, Barcelona, Spain

²⁵Department of Clinical Pathology, Robert-Bosch-Krankenhaus, and Dr. Margarete Fischer-Bosch Institute of Clinical Pharmacology, Stuttgart, Germany

²⁶Institute of Pathology, Eberhard-Karls-University of Tübingen, Tübingen, Germany

²⁷Laboratory of Pathology, Center for Cancer Research, National Cancer Institute, National Institutes of Health, Bethesda, USA

²⁸University of Barcelona, Barcelona, Spain

*these authors have contributed equally.

#these authors have contributed equally.

Running head: IGK/L enhancer hijacking in MCL

Scientific category: Lymphoid Neoplasia

Word Count: Abstract: 249, **Main Text:** 3985

Figures: 5, **Tables:** 1, **References:** 51

Suppl. Material: 1 pdf and 1 excel spreadsheet

Send correspondence to:

Sílvia Beà, Institut d'Investigacions Biomèdiques August Pi i Sunyer (IDIBAPS), Rosselló 149-153, Barcelona, 08036, Spain, Tel: +34-93-2275400 ext. 4792; E-mail: sbea@clinic.cat

KEY POINTS

1. Selective cryptic insertions of IG light chain enhancers activate *CCND2* and *CCND3* in cyclin D1⁻ mantle cell lymphomas
2. Most cyclin D1⁻ mantle cell lymphomas had *CCND2* or *CCND3* rearrangements whereas a small subset show upregulation of *CCNE1* and *CCNE2*

ABSTRACT

Mantle cell lymphoma (MCL) is characterized by the t(11;14)(q13;q32) translocation resulting in overexpression of cyclin D1. However, a small subset of cyclin D1-negative MCL (cyclin D1⁻ MCL) has been recognized, and approximately half of them harbor *CCND2* translocations while the primary oncogenic event in cyclin D1⁻/D2⁻ MCL remains elusive. To identify other potential mechanisms driving MCL pathogenesis we investigated 56 cyclin D1⁻/SOX11⁺ MCL by fluorescence *in situ* hybridization (FISH), whole genome/exome sequencing, gene expression and copy number arrays. FISH with break-apart probes identified *CCND2* rearrangements in 39 (70%) cases but not *CCND3* rearrangements. We analyzed 3 of these negative cases by whole-genome/exome sequencing and identified IGK (n=2) and IGL (n=1) enhancer hijackings near *CCND3* that were associated with cyclin D3 overexpression. By specific FISH probes, including the IGK enhancer region, we detected 10 additional cryptic IGK juxtapositions to *CCND3* (6 cases) and *CCND2* (4 cases) in MCL that overexpressed, respectively, these cyclins. A minor subset of 4 cyclin D1⁻ MCL cases lacked cyclin D rearrangements and showed upregulation of *CCNE1* and *CCNE2*. These cases had blastoid morphology, high genomic complexity, and *CDKN2A* and *RBI* deletions. Both genomic and gene expression profiles of cyclin D1⁻ MCL cases were indistinguishable from cyclin D1⁺ MCL. In conclusion, virtually all cyclin D1⁻ MCL carry *CCND2/CCND3* rearrangements with IG genes, including a novel IGK/L enhancer hijacking mechanism. A subset of cyclin D1⁻/D2⁻/D3⁻ MCL with aggressive features have cyclin E dysregulation. Specific FISH probes may allow the molecular identification and diagnosis of cyclin D1⁻ MCL.

INTRODUCTION

Mantle cell lymphoma (MCL) is a mature B-cell malignancy genetically characterized by the primary translocation t(11;14)(q13;q32) found in the vast majority cases.¹⁻³ This translocation juxtaposes the *CCND1* gene to an enhancer of the immunoglobulin heavy chain gene (IGH) leading to constitutive cyclin D1 upregulation. Nevertheless, a small subset of MCL lacks cyclin D1 overexpression and the t(11;14) (cyclin D1⁻ MCL).⁴⁻¹⁰ These cases have similar morphology, phenotype, gene expression profile, genomic alterations, and clinical behavior as conventional cyclin D1⁺ MCL.^{5,11,12} SOX11 is a transcriptional factor constantly overexpressed in most MCL independently of the expression of cyclin D1 and, therefore, it is a useful marker to recognize cyclin D1⁻ MCL cases.¹¹

Interestingly, the first six cyclin D1⁻ MCL identified in the Lymphoma/Leukemia Molecular Profiling Project showed overexpression of cyclin D2 or cyclin D3, but evidence of chromosomal rearrangements affecting these loci was not found by fluorescence *in situ* hybridization (FISH) using break-apart probes.⁴ However, different reports have detected occasional cyclin D1⁻ MCL cases with high levels of cyclin D2 due to chromosomal translocations with IG genes i.e. t(2;12)(p11;p13) [*IGK/CCND2*],^{6,8} t(12;22)(p13;q21) [*CCND2/IGL*],⁷ and a t(12;14)(p13;q32) [*CCND2/IGH*].⁹ In the largest series of cases analyzed, we identified 55% cases (22/40) with *CCND2* rearrangement, preferentially with IG light chains (68%), but *CCND3* rearrangement was not identified in the remaining cases using standard break-apart probes.⁵ So far, only one single MCL case with *CCND3/IGH* rearrangement has been reported.⁸

Overall, the potential role of *CCND2* and *CCND3* translocations as alternative pathogenic mechanisms to *CCND1* rearrangement in cyclin D1⁻ MCL are not yet fully understood, since not all reports of rearrangements were coupled with expression studies of the rearranged cyclins or with SOX11 expression. In order to clarify the genetic mechanisms behind cyclin D1⁻ MCL we performed an integrative analysis including a complete FISH panel, next-generation sequencing, gene expression, and copy number arrays, in a large series of well characterized cyclin D1⁻ MCL.

METHODS

Patients and samples

A total of 56 cyclin D1⁻ MCL cases (28 partially investigated in previous studies)^{4,5} were included in the current project based on i) morphology and phenotype consistent with MCL (CD5+ and CD23-); ii) absence of cyclin D1 expression and t(11;14)(q13;q32); and iii) SOX11 expression. The main clinicopathological and molecular features of the patients are described in **Table 1**. DNA/RNA extraction was performed from formalin-fixed and paraffin-embedded (FFPE) tissue blocks in 52 samples, fresh-frozen material in 7 samples, and Carnoy fixed cells in 2 samples. The study was approved by the Institutional Review Board of the Hospital Clinic of Barcelona.

Cytogenetic analyses

FISH analyses were performed on FFPE tissue sections or fixed cells from cytogenetic cultures. The FISH panel used to interrogate breaks and juxtapositions of the loci *CCND2*, *CCND3*, *CCNE1*, *CCNE2*, *IGH*, *IGL*, and *IGK* including both commercial and BAC-labeled probes is detailed in **Supplemental Table S1**. The extraction and labeling of BAC and PAC DNA, preparation of slides and hybridization was performed according to standard procedures.¹³ Each clone was first tested individually by hybridization on normal metaphases. Hybridizations were analyzed using standard fluorescence microscopes (Nikon Eclipse 50i or Zeiss) equipped with appropriate filter sets. Acquisition and processing of digital images were performed using the ISIS FISH Imaging System (MetaSystems, Altlußheim, Germany). For the detection of *IGK* cryptic insertions 2 overlapping BAC clones covering the *IGK* enhancer region were selected, labeled, and hybridized together with *CCND2*, *CCND3*, *CCNE1*, or *CCNE2* specific probes with different fluorochromes. Negative tissue controls for these FISH experiments included 1 reactive lymph node, four chronic lymphocytic leukemias (CLL), 6 diffuse large B-cell lymphomas (DLBCL), 1 follicular lymphoma (FL), and 1 splenic marginal zone lymphoma (SMZL). To verify *CCNE2* gain we used simultaneously *CCNE2* (8q22) and chr8 centromeric probes. Conventional cytogenetics was performed on G-banded chromosomes and results were described according to An International System for Human Cytogenomic Nomenclature (ISCN).¹⁴

Next-generation sequencing (NGS) analyses

Somatic structural variants (SVs) were analyzed by different NGS approaches in 5 MCL cases: long-insert-size (7-10Kb) paired-end mapping whole-genome sequencing (MP-WGS) of 4 tumors and 10 normal unmatched DNA; paired-end whole-genome sequencing (WGS) of tumor and matched normal sample of 1 patient; and whole-exome sequencing (WES) in 3 tumors (**Supplemental Figure S1**).^{15,16} Libraries were constructed according to standard protocols (Illumina) and sequencing was performed with an Illumina HiSeq 2000 instrument.¹⁵ Reads were mapped to hg19 human reference genome using the Burrows-Wheeler Aligner (BWA-MEM version 0.7.5a-r405). PCR duplicates were removed using MarkDuplicates algorithm from Picard tools. SVs were analyzed using different pipelines: i) BWA with the samse option was used for MP-WGS analysis in combination with custom scripts to detect interchromosomal translocations supported by at least four reads, followed by visual inspection; ii) Smufin¹⁷ and Lumpy¹⁸ were used to detect SVs in the WGS of case ID73; and iii) custom scripts were used to analyze/confirm potential interchromosomal SVs in the WES data. We excluded SVs in repetitive or ambiguously aligned regions in the MP-WGS analysis. Due to the lack of germline DNA for most samples, SVs present both in 2 or more of the 4 MP-WGS and 1 or more of 10 normal samples were removed as potential germline variants/artifacts. In case ID73, copy number alterations (CNA) from WGS were analyzed using FREEC¹⁹ and ASCAT algorithms, whereas single nucleotide variants (SNV) and indels were analyzed using 3 different pipelines: Smufin,¹⁷ Sidrón,²⁰ and Mutect2,²¹ and annotated by Annovar. Sanger sequencing for breakpoints detected by MP-WGS and/or WES data was performed using the primers detailed in **Supplemental Table S2**.

Gene expression and copy number analyses

Total RNA from 14 cyclin D1⁻ MCL and 7 cyclin D1⁺ MCL was extracted from FFPE tissue biopsies, processed using SensationPlus™ FFPE Amplification and 3' IVT Labelling Kit, and hybridized on GeneChip Human Genome U133 Plus 2.0 Arrays (Thermo Fisher Scientific, Waltham, MA, USA). Arrays were washed and stained using GeneChip Fluidics Station 450 (Thermo Fisher Scientific) and GeneChip Scanner. Limma²² was used to detect differentially expressed probesets and *P*-values were adjusted by the Benjamini-Hochberg method. In 38 cyclin D1⁻ MCL, 4 CLL, and 16 normal

samples gene expression levels of *CCND2*, *CCND3*, *CCNE1*, and *CCNE2* were investigated by quantitative PCR (qPCR) as previously described,⁵ using *GUSB* as endogenous control and Universal Human Reference RNA as a calibrator (**Supplemental Table S3**). Cyclin E1 protein expression was analyzed by immunohistochemistry (Santa Cruz Biotechnology, antibody clone sc-247, dilution 1:100) in 12 cyclin D1⁻ MCL, 1 CLL, 2 SMZL, and in control tissues (testis as positive control and tonsil and reactive lymph node as negative controls). CNA were evaluated in 42 cyclin D1⁻ cases (47 samples) with different approaches including: CGH-array Agilent 1M (Agilent, Santa Clara, CA), and SNP-arrays 500K, SNP6.0, or Oncoscan CNV (Thermo Fisher Scientific). CNA analysis was performed using Nexus Biodiscovery version 9.0 software (Biodiscovery, Hawthorne, CA, USA) as previously described.^{5,16} All cases were visually inspected by at least two independent observers.

RESULTS

Identification of cryptic rearrangements of IGK and IGL enhancer regions and cyclin D genes in cyclin D1⁻ MCL

To understand the molecular alterations present in cyclin D1⁻ MCL cases, we initially performed FISH analysis using *CCND2*, IGH, IGK, and IGL break-apart probes in 56 cyclin D1⁻ MCL and identified 39 (70%) cases with *CCND2* rearrangements (cyclin D2⁺ MCL), preferentially involving light chains IGK (55%) and IGL (13%) (**Supplemental Figure S1**). The remaining 17 patients (30%) without *CCND2* rearrangements were analyzed using a *CCND3* break-apart FISH probe but none of them showed rearrangements. Detailed FISH results of all cases are listed in **Supplemental Table S4**.

To investigate the presence of potential rearrangements that might have been undetectable by standard FISH approaches we performed MP-WGS in 2 cases that were negative for FISH rearrangements of *CCND2* and *CCND3* (ID3 and ID6). We detected several somatic interchromosomal SVs (4 in ID3 and 7 in ID6) (**Figure 1A** and **Supplemental Table S5**). Strikingly, both cases showed a similar rearrangement involving IGK in chromosome 2 and *CCND3* in chromosome 6, which consisted of a small insertion (26.6 Kb for ID3 and 27.3 Kb for ID6) including the IGK enhancer. Virtually the entire IGK enhancer (26.4 Kb), as defined by chromatin states in normal

mature B-cells,²³ was integrated upstream of the *CCND3* gene (8.4 kb upstream in case ID6 and 65 kb in case ID3). We confirmed these cryptic insertions by Sanger sequencing in both cases and we could identify the breakpoint at single nucleotide resolution (**Figure 1B**). This insertion was also observed by WES in case ID3. In addition, we validated these findings by FISH in case ID3 using a new combination of fusion probes, one covering the *CCND3* gene and the other including the enhancer of IGK (IGK-enh) (**Figure 1C**). Additionally, WES analysis of case ID5 (also negative for FISH with *CCND3* break-apart probe) revealed a similar cryptic insertion of the IGL enhancer region in chromosome 22 near the 3' of *CCND3* gene, which was further verified by Sanger sequencing (**Figure 1B**). Interestingly, those 3 cases (ID3, ID5, and ID6) in which we identified the cryptic IGK/L enhancer and *CCND3* rearrangement (enhancer hijacking) were initially reported to have cyclin D3 overexpression by microarray expression analysis,⁴ highlighting the functional impact of the cryptic rearrangement at mRNA level, and the potential utility of cyclin D2/D3 expression to help to identify these tumors with cryptic rearrangements in the absence of conventional translocation of the cyclins.

In addition, we performed MP-WGS of case ID76, positive for the IGK/*CCND2* rearrangement by FISH and also by karyotype. We detected 23 interchromosomal SVs, including two which confirmed the IGK/*CCND2* reciprocal translocation. Interestingly, the MP-WGS coupled with SNP6.0 array data allowed to refine several alterations of the karyotype (**Figure 2** and **Supplemental Table S5**).

Identification of additional cryptic IGK/*CCND3* and IGK/*CCND2* by FISH

The finding of this enhancer hijacking phenomenon in cyclin D1⁻ MCL leading to overexpression of *CCND3* prompted us to explore the expression of all cyclins of the G1 phase of cell cycle (*CCND2*, *CCND3*, *CCNE1*, and *CCNE2*) in cyclin D1⁻ MCL, CLL, and non-neoplastic samples (reactive lymph nodes and tonsils) by qPCR. As expected, all *CCND2*-rearranged cases tested (n=24) (cyclin D2⁺ MCL) showed elevated levels of *CCND2* (median *CCND2* expression=127.5) compared to non-rearranged *CCND2* MCL cases (median 7.0)($P<.001$) (**Figure 3**). Interestingly, among the 14 cases tested without *CCND2* or *CCND3* rearrangements, 6 cases overexpressed *CCND3* (median 18.9), 4 cases overexpressed *CCND2* (median 66.2), and the remaining 4 cases overexpressed

concomitantly *CCNE1* along with *CCNE2* (median 7.6 and 3.8, respectively) (**Table 1**, **Figure 3**, and **Supplemental Figure S1**).

Given the high levels of *CCND3* in these additional 6 cyclin D1⁻ MCL cases, we explored the presence of similar cryptic IGK and *CCND3* juxtapositions by FISH using the IGK-enh and *CCND3* fusion probe. We detected fusion IGK/*CCND3* signals in all 6 cases (**Supplemental Figure S2A** and **Supplemental Table S4**), but not in any of the 9 control samples tested. The presence of these cryptic IG insertions near *CCND3* gene leading to *CCND3* overexpression prompted us to hypothesize that the remaining 4 cases with high levels of *CCND2* expression (and negative for *CCND2* breaks using break-apart FISH probes) could present similar cryptic aberrations. Thus, we performed FISH using IGK-enh and *CCND2* probes and we could detect the juxtaposition of both signals in all 4 cases (**Supplemental Figure S2B-C** and **Supplemental Table S4**), but not in the 9 controls tested. Together, these data show that 13 out of the 17 (76%) MCL negative for *CCND2/D3* rearrangements using break-apart probes had IGK/L-enhancer hijacking into either *CCND3* (9 cases) or *CCND2* (4 cases).

Absence of detectable primary genetic events in a small subset of cyclin D1⁻ MCL

After the identification of the cryptic IGK enhancer rearrangements with *CCND3* and *CCND2* in MCL negative for the *CCND2/D3* break-apart by FISH, only 4 of the 56 cyclin D1⁻ MCL remained without an identified primary genetic event. All 4 cases overexpressed concomitantly *CCNE1* and *CCNE2* mRNA but not the remaining cyclin D genes. We performed cyclin E1 immunohistochemistry and the 3 cases tested (ID26, ID73, and ID77) were strongly positive in most of the cells (~65%) (**Figure 4A**) as compared to only 1 out of 9 cyclin D2⁺ or cyclin D3⁺ MCL, 1 out of 3 B-cell lymphomas (a SMZL sample), and none of the 2 non-malignant lymphoid tissues tested. These findings confirmed the cyclin E1 overexpression also at protein level in these cases. To determine whether the mRNA and protein overexpression could be due to a genomic rearrangement, we performed FISH using a *CCNE1* break-apart probe in 3 cases but none of them showed a signal constellation suggestive of *CCNE1* reorganization. Furthermore, these cases showed no evidence of IGK, IGL, and IGH rearrangement by FISH. In order to test for potential cryptic insertion of IGK enhancer in *CCNE1* or *CCNE2* loci, we

performed FISH in the 3 cases and none of them showed a rearrangement or gain in *CCNE1* or *CCNE2* (**Supplemental Table S4**).

We then performed MP-WGS (tumor) and WGS (tumor and normal) of the remaining case with *CCNE1/E2* overexpression and lack of FISH analysis (case ID73) (**Figure 4B** and **Supplemental Table S6**). We could not find any genetic rearrangement involving IG, cyclin D or cyclin E genes. Of note, we detected a 8q21.2-q23 high-level gain (around 6 copies estimated by WGS) which included the *CCNE2* locus (**Figure 4C**), this was confirmed by FISH, that showed at least *CCNE2* 4 signals per cell (**Figure 4D**). In addition, we observed 32 intrachromosomal and 35 interchromosomal rearrangements (12 only detected by the MP-WGS strategy), and 2 homozygous deletions, one truncating *RBI* at 13q14 and one affecting *CDKN2A* at 9p21. We also analyzed the genes truncated by SVs and found disruption of 50 genes, including cancer-associated genes such as *NBN*, *BCL2L11* (*BIM*), and *ARID1B* among others. We detected 32 somatic protein-coding mutations by WGS analysis, none of them previously reported in MCL samples (**Figure 4B** and **Supplemental Table S7**).^{16,24} The tumor purity of the case inferred by ASCAT was 78.2% and the ploidy 2.13 (diploid).

Global expression, genomic profiles, and overall survival in cyclin D1⁻ MCL

In order to compare the global gene expression profile of 14 cyclin D1⁻ MCL with 7 conventional cyclin D1⁺ MCL we performed unsupervised clustering analysis and observed that the cases did not segregate into different clusters. Moreover, principal component analysis showed that the main source of variability (45.3% of the variability) was not related to the absence of cyclin D1 expression (**Supplemental Figure S3**). As expected, *CCND1* was the only significant differentially expressed gene (adjusted $P=2.3 \times 10^{-11}$), and besides occasional cases with *CCND2* overexpression (10 cases), *CCND3* overexpression (one case), or concomitant *CCNE1/CCNE2* (2 cases), no other overexpressed genes were found, including those recurrently translocated and upregulated in other B-cell neoplasms.

Finally, we compared the global profile of CNA of 42 cyclin D1⁻ MCL with those of 116 previously published cyclin D1⁺/SOX11⁺ MCL cases.^{12,16,25} The profiles of CNA were indistinguishable, and cyclin D1⁻ MCL cases had a high complex profile of alterations with a median 10 CNA/case, frequent deletions of 9p21/*CDKN2A* (48%),

11q22/*ATM* (33%), and 17p13/*TP53* (19%) (**Table 1**, **Figure 5**, and **Supplemental Figure S4A**, and **Supplemental Table S8**). No statistical differences were found between cyclin D2⁺ (n=29) vs cyclin D3⁺ (n=9) MCL subgroups (**Supplemental Figure S4B**). Interestingly, all 4 cases with *CCNE1/E2* overexpression showed alterations in cell cycle and apoptosis related-genes, such as focal homozygous deletions of 9p21 (*CDKN2A*), 13q14 deletions (*RBI*), and large high-copy gains of 18q (*BCL2*). These 4 cases also had a higher number of CNA (median 17 CNA/case) than cyclin D2⁺ MCL and cyclin D3⁺ MCL (median 9 CNA/case) (**Table 1**).

We also analyzed the CNA of 2 different tumor samples of the same patient in 5 cases (1 synchronous and 4 sequential) and they showed both common and unique alterations, suggesting the presence of genetically heterogeneous subpopulations and clonal evolution in each case (**Supplemental Figure S4C**).

The cyclin D1⁻ MCL patients had a similar overall survival (OS) than cyclin D1⁺/*SOX11*⁺ MCL (**Supplemental Figure S5A**).²⁶ Noteworthy, although the 3-year OS was higher in patients with cyclin D3⁺ than patients with cyclin D2⁺ or cyclin E⁺ (100%, 59% and 75%, respectively), these differences were not statistically significant (**Table 1** and **Supplemental Figure S5B**).

DISCUSSION

MCL is a well characterized lymphoid neoplasm with the t(11;14) leading to cyclin D1 overexpression as the primary genetic event. However, a particular subset of cases with the same histology and phenotype but lacking cyclin D1 expression has been recognized.¹ We previously reported balanced chromosomal translocations of *CCND2* locus with IG genes in approximately half of these cases and emphasized the value of this approach for the recognition of a proportion of cyclin D1⁻ MCL.⁵ Nevertheless, the primary rearrangement in the remaining cases could not be established. We document here a deep comprehensive analysis of the largest series of cyclin D1⁻ MCL cases ever reported, integrating molecular and genetic data with NGS technologies, which allowed us to unveil for the first time selective cryptic insertions of IGK/L enhancer regions (enhancer hijacking) into cyclin D genes in the majority of the cases that lacked a *CCND2* conventional rearrangement.

With our integrative study we found that 16% of cyclin D1⁻ MCL had *CCND3* rearrangements, all of them consisting of a cryptic insertion of the IGK/L enhancer. These rearrangements led to *CCND3* overexpression and may be considered as an alternative molecular mechanism to *CCND1* or *CCND2* primary translocations. Interestingly, a *CCND3/IGH* translocation has been previously reported in one MCL,⁸ one low grade B-cell lymphoma, 3 splenic lymphomas, and 7 aggressive B-cell lymphomas.²⁷⁻³⁰ Notably, in all these cases the *CCND3* rearrangement was with IGH and detectable by conventional cytogenetics. Intriguingly, some of these cases expressed CD5, had blastoid morphology and unmutated-IGHV with splenic and leukemic involvement. Although SOX11 expression was not studied, these features suggest that at least some of these cases could correspond to MCL. In multiple myeloma, 15-25% cases have *CCND1/IGH* rearrangement or *CCND1* gain/amplification coupled with *CCND1* overexpression, 3-5% have *CCND3/IGH* rearrangement associated with *CCND3* overexpression, whereas *CCND2* overexpression has been detected in a subset of 5% cases without apparent genomic alterations.^{31,32} Interestingly, no *CCND3* rearrangement with IGK has been previously detected in human lymphomas, but the application of RNA-seq analyses of a canine DLBCL showed the presence of an IGK/*CCND3* rearrangement associated with overexpression of *CCND3*.³³

In our series of cyclin D1⁺ MCL a large proportion of cases harbor conventional *CCND2* rearrangements (70%), a higher frequency than the previously reported (55%).⁵ We have now identified an additional subset of 7% cases with cryptic IGK/*CCND2*, thus, increasing the overall frequency of *CCND2* rearrangement to 77%. Interestingly, *CCND2* is preferentially rearranged with IG light chains genes instead of IGH, being IGK more frequent than IGL (83% and 17%). Similarly, 8 *CCND3* rearrangements were with IGK, only one with IGL, and none with IGH. Of note, both *CCND2* and *CCND3* chromosomal breaks occur in a large region (including the 5' or 3' of *CCND3*) whereas the IGK breaks occur in a restricted region which contained the enhancer element.

One of the most remarkable findings in our study was the restricted small insertion of the IGK/L enhancer close to the *CCND2/D3* genes leading to their respective overexpression, a finding not previously detected in lymphoid neoplasms. We could resolve the breakpoints at single nucleotide resolution identifying 1-3 identical nucleotides on both sides of the breakpoints. These special enhancer rearrangements seem to parallel the mechanism of enhancer hijacking activating known oncogenes recently identified in solid tumors and some lymphoid neoplasms. In solid tumors, recurrent SVs bring together a distal active enhancer to an oncogene promoting its expression. This mechanism has been identified for *MYC* and *MYCN* in high-risk pediatric neuroblastoma,³⁴ *TERT* in neuroblastoma,³⁵ *PRDM6*,³⁶ *GFII*, *GFIIIB* and *DDX31*^{37,38} in medulloblastoma, and *IGF2* in colorectal cancer.³⁹ *MYC* rearrangements with super-enhancers from non-IG genes (i.e. *NSMCE2*, *TXNDC5*, *FAM46C*, *FOXO3*, *PRDMI*) have been frequently found in multiple myeloma.⁴⁰ In addition to translocations, lymphoid neoplasms may have other small-scale SV involving active enhancers such as amplifications of enhancer regions close to oncogenes or selective deletions and inversions that reposition candidate enhancer elements in the vicinity of oncogenes.^{41,42} All these findings emphasize that SVs targeting active enhancer regions may be a mechanism of activating oncogenes more prevalent than initially thought and present across different cancer types. It will be interesting to explore whether the “IG enhancer insertions” identified here may also affect other oncogenes such as *MYC*, *BCL2* or *CCND1* in B-cell lymphomas with high mRNA or protein expression but not carrying the canonical translocations.

In the present study we demonstrated that 93% of cyclin D1⁻ MCL have *CCND2* or *CCND3* rearrangements. However, a small number of cases (n=4), representing 7% of cyclin D1⁻ MCL, lacked a genetic alteration and overexpression of these cyclins, despite having the morphology and phenotype of MCL. In this minority of cases we observed overexpression of *CCNE1* and *CCNE2* but without a primary structural rearrangement. The expression levels of these cyclins, although significantly higher than in other MCL and controls, were relatively moderate, not suggestive of being triggered by a translocation. In addition, all 4 cases showed concomitantly similar levels of both *CCNE1* and *CCNE2* genes, located in different chromosomes. The mechanism/s leading to their concomitant upregulation in these cases are unclear. Only one of the cases had a high-copy gain of *CCNE2* gene (located at 8q22.1) but no concomitant gain of *CCNE1* (located at 19q12), and these 2 genomic regions were not gained/amplified in the remaining cases. A potential explanation could be that these cases may have an upstream common dysregulation mechanism. In contrast to cyclin D genes, the rearrangement of *CCNE1* in B-cell neoplasms is exceptionally rare with only a single reported case of DLBCL with *IGH/CCNE1* rearrangement and cyclin E1 protein overexpression.⁴³ Another feature of the 4 cyclin E⁺ MCL was a high genomic complexity, which is in line with previously reported *CCNE1* dysregulation (by locus amplification and/or overexpression) in solid tumors, associated with chromosome instability and aggressive behavior.⁴⁴⁻⁴⁷ The lack of overexpression of classic cyclin Ds in these 4 cases may make their classification as MCL debatable. However, the pathological features with classical or blastoid morphology, CD5 and SOX11 expression, deletions of *CDKN2A* and *RBI*, and aggressive clinical course, suggest that these tumors are closer to MCL than to other mature B-cell neoplasms. Further studies are needed to confirm the most appropriate taxonomy of these uncommon cases.

Overall, we show that cyclin D1⁻ and cyclin D1⁺ MCL share a common expression and genomic profile as well as clinical outcome.^{26,48} Our results highlight that *CCND2*, *CCND3*, and possibly also *CCNE1* and *CCNE2*, may be *bona fide* alternative alterations to *CCND1* in MCL pathogenesis, that, together with SOX11 overexpression, may represent the main oncogenic initial hits in MCL.⁴⁹ However, among the 3 subgroups of cyclin D1⁻ MCL there are some peculiarities: i) the levels of *CCND2* in *CCND2*-rearranged cases were very high and comparable to those of *CCND1* in MCL with the t(11;14), whereas the levels of *CCND3* in the *CCND3*-rearranged cases were moderate (one order of magnitude lower). The differences in levels of expression of

cyclin genes may have biologic and clinical implications, similar to what occurs in the conventional MCL cases with high or low *CCND1* levels, where high levels of *CCND1* have been associated with high proliferation and worse survival;^{50,51} ii) MCL with *CCND3* gene rearrangements lacked high-risk genetic alterations such as *TP53* deletions and showed low frequency of *CDKN2A* deletion; iii) *CCNE1/E2* expression, although moderate, was associated with blastoid morphology, high genomic complexity, high proliferation, and short survival, consistent with the role of these cyclins as potent oncogenes,⁴⁴ compared to the weak oncogenic potential of cyclin D genes.

In conclusion, using an integrative molecular and genetic analysis we have identified IG light chain enhancer hijacking next to *CCND2* or *CCND3* genes as a novel oncogenic driver in 23% of cyclin D1⁻ MCL. We also recognized a small subset of aggressive cyclin D1⁻ MCL carrying cyclin E dysregulation. In addition to the pathogenic significance of these findings, the approach used here may be useful for the diagnosis of these tumors.

Acknowledgement: This work was supported by research funding from Fondo de Investigaciones Sanitarias, Instituto de Salud Carlos III PI14/00571 and PI17/01061 (SB), Fundació La Marató de TV3-Càncer/2013410 (SB), Fundació Crèdit Andorrà, Ministerio de Economía y Competitividad, SAF2015-64885-R (EC), SAF2017-87811-R (XSP) from Plan Nacional de I+D+I, Generalitat de Catalunya Suport Grups de Recerca 2014-SGR-378 (SB), 2017-SGR-1142 (EC), and the European Regional Development Fund “Una manera de fer Europa”, CERCA Programme/Generalitat de Catalunya. EC is an Academia Researcher of the "Institució Catalana de Recerca i Estudis Avançats" of the Generalitat de Catalunya. Personal staff (Miriam Prieto and Noelia García) are supported by "Acció instrumental d'incorporació de científics i tecnòlegs PERIS 2016" (SLT002/16/00347 and SLT002/16/00336 from Generalitat de Catalunya). Thanks to: the Hematopathology Collection for sample procurement; Silvia Martín, Noelia García, Candida Gómez, Cristina Capdevila, and Maria Rodríguez-Rivera for excellent technical assistance; the Molecular Cytogenetic Platform of IMIM, Hospital del Mar (Barcelona) for providing BAC clones and the support of the technical staff of the molecular cytogenetic laboratories of the Institutes of Human Genetics in Kiel and Ulm. Thanks to contributors of individual cases: Iwona Wlodarska (Leuven, Belgium), Philippe Gaulard (Creteil, France), Wendy Erber (Crawley, Australia), Pilar Forcada (Terrassa, Spain), Grevelyn Sosa Rotundo (Madrid, Spain), Alejandra Carvajal (San Jose, Costa Rica), Camille Gonzalez (New York, US), Nhora Silva Perez (Cali, Colombia); Lluís Rodríguez (Vic, Spain). The arrays were performed at qGenomics (www.qgenomics.com), CeGen (PTI3/0001, ISCHIII-SGEFI/FEDER), and IDIBAPS Genomics core facility. This work was developed at the Centro Esther Koplowitz (CEK), Barcelona, Spain.

Author Contributions: E.C., S.Bea designed the study; D.M-G., R.V-M., J.G-A., D.T., S.Bel., C.L-O., X-S.P., S.Bea analyzed and interpreted NGS data; A.N., M.P., R.W., G.R., S.Ben., B.E., D.C., R.S., S.Bea performed and interpreted cytogenetic analysis; D.M-G., A.N., M.P., I.S., S.Bea performed and interpreted molecular studies; G.C. performed statistical analyses; I.R-C., G.R., L.dL., A.R., J-A.F., E-D.-H., K.F., J.D., D.W., D.dJ., F.C., S.O'C., S-H.S., B-G.F., L.V., E.M., G.O., L.Q-M., E-S.J. and E.C. reviewed and collected IHC and pathological data; D.M-G., A.N., E.C., and SBea wrote the manuscript; S.B. directed and supervised the research. All authors approved the final manuscript.

Other Information: Sequencing, expression, and copy number array data have been deposited at the European Genome-Phenome Archive (EGA, <http://www.ebi.ac.uk/ega/>), which is hosted at the European Bioinformatics Institute (EBI), under accession number EGAS00001003058 (WGS and WES) and EGAS00001003060 (copy number and expression arrays). Copy number arrays of the cases included in Salaverria *et al* Blood 2013 had been previously deposited in Gene Expression Omnibus (GEO) under accession number GSE42854.

Conflict-of-interest disclosure: EC has received research funding from Gilead Sciences, and has been consultant for Takeda, Celgene and Gilead, and is author in a Lymphoma and Leukemia Molecular Profiling Project (LLMPP) patent "Method for selecting and treating lymphoma types" PCT/US14/64161.

REFERENCES

1. Swerdlow SH, Campo E, Harris N et al. (Eds.): WHO Classification of Tumours of Haematopoietic and Lymphoid Tissues. IARC: Lyon 2017.
2. Jares P, Colomer D, Campo E. Molecular pathogenesis of mantle cell lymphoma. *J.Clin.Invest* 2012;122:3416-3423.
3. Royo C, Salaverria I, Hartmann EM et al. The complex landscape of genetic alterations in mantle cell lymphoma. *Semin.Cancer Biol.* 2011;21:322-334.
4. Fu K, Weisenburger DD, Greiner TC et al. Cyclin D1-negative mantle cell lymphoma: a clinicopathologic study based on gene expression profiling. *Blood* 2005;106:4315-4321.
5. Salaverria I, Royo C, Carvajal-Cuenca A et al. CCND2 rearrangements are the most frequent genetic events in cyclin D1(-) mantle cell lymphoma. *Blood* 2013;121:1394-1402.
6. Gesk S, Klapper W, Martin-Subero JI et al. A chromosomal translocation in cyclin D1-negative/cyclin D2-positive mantle cell lymphoma fuses the CCND2 gene to the IGK locus. *Blood* 2006;108:1109-1110.
7. Shiller SM, Zieske A, Holmes H, III et al. CD5-positive, cyclinD1-negative mantle cell lymphoma with a translocation involving the CCND2 gene and the IGL locus. *Cancer Genet.* 2011;204:162-164.
8. Wlodarska I, Dierickx D, Vanhentenrijk V et al. Translocations targeting CCND2, CCND3, and MYCN do occur in t(11;14)-negative mantle cell lymphomas. *Blood* 2008;111:5683-5690.
9. Herens C, Lambert F, Quintanilla-Martinez L et al. Cyclin D1-negative mantle cell lymphoma with cryptic t(12;14)(p13;q32) and cyclin D2 overexpression. *Blood* 2008;111:1745-1746.
10. Quintanilla-Martinez L, Slotta-Huspenina J, Koch I et al. Differential diagnosis of cyclin D2+ mantle cell lymphoma based on fluorescence in situ hybridization and quantitative real-time-PCR. *Haematologica* 2009;94:1595-1598.
11. Mozos A, Royo C, Hartmann E et al. SOX11 expression is highly specific for mantle cell lymphoma and identifies the cyclin D1-negative subtype. *Haematologica* 2009;94:1555-1562.
12. Hartmann EM, Campo E, Wright G et al. Pathway discovery in mantle cell lymphoma by integrated analysis of high-resolution gene expression and copy number profiling. *Blood* 2010;116:953-961.
13. Ventura RA, Martin-Subero JI, Jones M et al. FISH analysis for the detection of lymphoma-associated chromosomal abnormalities in routine paraffin-embedded tissue. *J.Mol.Diagn.* 2006;8:141-151.

14. ISCN 2016: McGowan-Jordan, J., Schmid, M. (2016), ISCN 2016: An International System for Human Cytogenomic Nomenclature. S. Karger, Basel.
15. Puente XS, Bea S, Valdes-Mas R et al. Non-coding recurrent mutations in chronic lymphocytic leukaemia. *Nature* 2015;526:519-524.
16. Bea S, Valdes-Mas R, Navarro A et al. Landscape of somatic mutations and clonal evolution in mantle cell lymphoma. *Proc.Natl.Acad.Sci.U.S.A* 2013;110:18250-18255.
17. Moncunill V, Gonzalez S, Bea S et al. Comprehensive characterization of complex structural variations in cancer by directly comparing genome sequence reads. *Nat.Biotechnol.* 2014;32:1106-1112.
18. Layer RM, Chiang C, Quinlan AR, Hall IM. LUMPY: a probabilistic framework for structural variant discovery. *Genome Biol.* 2014;15:R84.
19. Boeva V, Zinovyev A, Bleakley K et al. Control-free calling of copy number alterations in deep-sequencing data using GC-content normalization. *Bioinformatics.* 2011;27:268-269.
20. Puente XS, Pinyol M, Quesada V et al. Whole-genome sequencing identifies recurrent mutations in chronic lymphocytic leukaemia. *Nature* 2011;475:101-105.
21. Cibulskis K, Lawrence MS, Carter SL et al. Sensitive detection of somatic point mutations in impure and heterogeneous cancer samples. *Nat.Biotechnol.* 2013;31:213-219.
22. Smyth GK. Linear models and empirical bayes methods for assessing differential expression in microarray experiments. *Stat.Appl.Genet.Mol.Biol.* 2004;3:Article3.
23. Beekman R, Chapaprieta V, Russinol N et al. The reference epigenome and regulatory chromatin landscape of chronic lymphocytic leukemia. *Nat.Med.* 2018;24:868-880.
24. Zhang J, Jima D, Moffitt AB et al. The genomic landscape of mantle cell lymphoma is related to the epigenetically determined chromatin state of normal B cells. *Blood* 2014;123:2988-2996.
25. Royo C, Navarro A, Clot G et al. Non-nodal type of mantle cell lymphoma is a specific biological and clinical subgroup of the disease. *Leukemia* 2012;26:1895-1898.
26. Clot G, Jares P, Gine E et al. A new molecular assay and genomic complexity predict outcome in conventional and leukemic non-nodal mantle cell lymphoma. *Blood* 2018
27. Sonoki T, Harder L, Horsman DE et al. Cyclin D3 is a target gene of t(6;14)(p21.1;q32.3) of mature B-cell malignancies. *Blood* 2001;98:2837-2844.

28. Watanuki J, Hatakeyama K, Sonoki T et al. Bone marrow large B cell lymphoma bearing cyclin D3 expression: clinical, morphologic, immunophenotypic, and genotypic analyses of seven patients. *Int.J.Hematol.* 2009;90:217-225.
29. Wren D, Walker BA, Bruggemann M et al. Comprehensive translocation and clonality detection in lymphoproliferative disorders by next-generation sequencing. *Haematologica* 2017;102:e57-e60.
30. Sole F, Espinet B, Salido M et al. Translocation t(6;14)(p12;q32): a novel cytogenetic abnormality in splenic lymphoma with villous lymphocytes. *Br.J.Haematol.* 2000;110:241-243.
31. Tian E, Sawyer JR, Heuck CJ et al. In multiple myeloma, 14q32 translocations are nonrandom chromosomal fusions driving high expression levels of the respective partner genes. *Genes Chromosomes.Cancer* 2014;53:549-557.
32. Fonseca R, Bergsagel PL, Drach J et al. International Myeloma Working Group molecular classification of multiple myeloma: spotlight review. *Leukemia* 2009;23:2210-2221.
33. Ulve R, Rault M, Bahin M et al. Discovery of human-similar gene fusions in canine cancers. *Cancer Res.* 2017;77:5721-5727.
34. Zimmerman MW, Liu Y, He S et al. MYC Drives a Subset of High-Risk Pediatric Neuroblastomas and Is Activated through Mechanisms Including Enhancer Hijacking and Focal Enhancer Amplification. *Cancer Discov.* 2018;8:320-335.
35. Valentijn LJ, Koster J, Zwijnenburg DA et al. TERT rearrangements are frequent in neuroblastoma and identify aggressive tumors. *Nat.Genet.* 2015;47:1411-1414.
36. Northcott PA, Buchhalter I, Morrissy AS et al. The whole-genome landscape of medulloblastoma subtypes. *Nature* 2017;547:311-317.
37. Northcott PA, Lee C, Zichner T et al. Enhancer hijacking activates GFI1 family oncogenes in medulloblastoma. *Nature* 2014;511:428-434.
38. Grobner SN, Worst BC, Weischenfeldt J et al. The landscape of genomic alterations across childhood cancers. *Nature* 2018;555:321-327.
39. Weischenfeldt J, Dubash T, Drainas AP et al. Pan-cancer analysis of somatic copy-number alterations implicates IRS4 and IGF2 in enhancer hijacking. *Nat.Genet.* 2017;49:65-74.
40. Affer M, Chesi M, Chen WG et al. Promiscuous MYC locus rearrangements hijack enhancers but mostly super-enhancers to dysregulate MYC expression in multiple myeloma. *Leukemia* 2014;28:1725-1735.
41. Chapuy B, Stewart C, Dunford AJ et al. Molecular subtypes of diffuse large B cell lymphoma are associated with distinct pathogenic mechanisms and outcomes. *Nat.Med.* 2018;24:679-690.

42. Ryan RJ, Drier Y, Whitton H et al. Detection of Enhancer-Associated Rearrangements Reveals Mechanisms of Oncogene Dysregulation in B-cell Lymphoma. *Cancer Discov.* 2015;5:1058-1071.
43. Nagel I, Akasaka T, Klapper W et al. Identification of the gene encoding cyclin E1 (CCNE1) as a novel IGH translocation partner in t(14;19)(q32;q12) in diffuse large B-cell lymphoma. *Haematologica* 2009;94:1020-1023.
44. Spruck CH, Won KA, Reed SI. Deregulated cyclin E induces chromosome instability. *Nature* 1999;401:297-300.
45. Hubalek MM, Widschwendter A, Erdel M et al. Cyclin E dysregulation and chromosomal instability in endometrial cancer. *Oncogene* 2004;23:4187-4192.
46. Alsina M, Landolfi S, Aura C et al. Cyclin E amplification/overexpression is associated with poor prognosis in gastric cancer. *Ann.Oncol.* 2015;26:438-439.
47. Scaltriti M, Eichhorn PJ, Cortes J et al. Cyclin E amplification/overexpression is a mechanism of trastuzumab resistance in HER2+ breast cancer patients. *Proc.Natl.Acad.Sci.U.S.A* 2011;108:3761-3766.
48. Rosenquist R, Bea S, Du MQ, Nadel B, Pan-Hammarstrom Q. Genetic landscape and deregulated pathways in B-cell lymphoid malignancies. *J.Intern.Med.* 2017;282:371-394.
49. Bea S, Amador V. Role of SOX11 and Genetic Events Cooperating with Cyclin D1 in Mantle Cell Lymphoma. *Curr.Oncol.Rep.* 2017;19:43.
50. Rosenwald A, Wright G, Wiestner A et al. The proliferation gene expression signature is a quantitative integrator of oncogenic events that predicts survival in mantle cell lymphoma. *Cancer Cell* 2003;3:185-197.
51. Scott DW, Abrisqueta P, Wright GW et al. New Molecular Assay for the Proliferation Signature in Mantle Cell Lymphoma Applicable to Formalin-Fixed Paraffin-Embedded Biopsies. *J.Clin.Oncol.* 2017;35:1668-1677.

Table 1. Clinicopathological and molecular features of the 56 cyclin D1⁻ MCL.
CI: confidence interval; CNA: copy number alterations; IHC: immunohistochemistry; qPCR:

Parameter	Total n=56 (%)	cyclin D2 ⁺ n=43 (%)	cyclin D3 ⁺ n=9 (%)	cyclin E ⁺ n=4 (%)	P- value
Median age (years)	65	66	60	75	0.161
Ratio male/female	2.4/1	3.2/1	2/1	0/1	0.029*
Growth pattern					1
Nodular and/or diffuse	50/52 (96%)	40/42 (95%)	6/6 (100%)	4/4 (100%)	
Mantle zone	2/52 (4%)	2/42 (5%)	0/6 (0%)	0/4 (0%)	
Morphology					0.029*
Classical	43 (81%)	34/40 (85%)	8/9 (89%)	1/4 (25%)	
Blastoid	10 (19%)	6/40 (15%)	1/9 (11%)	3/4 (75%)	
Expression (IHC)					
SOX11 positive	56 (100%)	43/43 (100%)	9/9 (100%)	4/4 (100%)	1
CD5 positive	54/55 (98%)	43/43 (100%)	7/8 (88%)	4/4 (100%)	0.218
CD23 negative	47/47 (100%)	36/36 (100%)	7/7 (100%)	4/4 (100%)	1
CD10 negative	39/39 (100%)	31/31 (100%)	4/4 (100%)	4/4 (100%)	1
Ki67 (≥30%)	24/42 (57%)	18/33 (55%)	2/5 (40%)	4/4 (100%)	0.153
Median expression (qPCR)					
CCND2	17.0	124.8	7.0	4.8	<0.001
CCND3	2.0	1.8	18.9	2.6	<0.001
CCNE1	1.0	1.1	0.9	7.6	0.009
CCNE2	0.8	0.8	0.6	3.8	0.077
Molecular					
Median CNA/case	10	9	9	17	0.098
Chromothripsis	10/42 (24%)	6/29 (21%)	3/9 (33%)	1/4 (25%)	0.847
-17p13/TP53	8/42 (19%)	8/29 (28%)	0/9 (0%)	0/4 (0%)	0.144
-11q22/ATM	14/42 (33%)	9/29 (31%)	5/9 (55%)	0/4 (0%)	0.140
-9p21/CDKN2A	20/42 (48%)	14/29 (48%)	2/9 (22%)	4/4 (100%)	0.033*
-13q14/RBI	17/42 (40%)	9/29 (31%)	4/9 (44%)	4/4 (100%)	0.030*
+18q	15/42 (36%)	8/29 (28%)	3/9 (33%)	4/4 (100%)	0.025*
+3q	23/42 (55%)	18/29 (62%)	3/9 (33%)	2/4 (50%)	0.378
-1p	16/42 (38%)	10/29 (34%)	6/9 (67%)	0/4 (0%)	0.049*
Clinical data					
Treated at diagnosis [#]	38/41 (93%)	27/29 (93%)	7/8 (88%)	4/4 (100%)	0.589
High-dose therapy (%)	2/41 (5%)	2/29 (7%)	-	-	
Immunochemotherapy (%)	25/41 (61%)	18/29 (62%)	3/8 (38%)	4/4 (100%)	
Other (%)	11/41 (27%)	7/29 (24%)	4/8 (50%)	-	
Observation (%)	3/41 (7%)	2/29 (7%)	1/8 (13%)	-	
3-yr overall survival (95 CI%)	68% (54-86)	59% (42-83)	100% (100-100)	75% (43-100)	0.424

quantitative PCR. *P-values below 0.05 were considered significant. P-values were calculated using the Fisher's exact and Kruskal-Wallis tests for categorical or continuous variables between the 3 groups, respectively. [#]High-dose therapy includes Cytarabine-based immunochemotherapy; Immunochemotherapy includes R-CHOP and R-CHOP-like regimens; and Other includes low-dose therapy (alkylating agents alone or in combination) and radiotherapy.

FIGURE LEGENDS

Figure 1. Cryptic insertions of IG light chain enhancer regions near *CCND3* gene in 3 cyclin D1⁻ MCL. (A) Circos plots with interchromosomal SVs detected by MP-WGS (black lines) and CNA detected by copy number arrays (blue for gains and red for losses) in cases ID6 and ID3. The rearrangement between chr2 (IGK-enh) and chr6 (*CCND3*) in both cases is indicated with a discontinuous line. (B) Schematic representation of the 6p region around *CCND3* locus showing the location of the cryptic insertion of the IGK enhancer (chr2) close to the 5' of *CCND3* gene in cases ID6 and ID3 (the length of the inserted fragments is indicated), and the location of the cryptic insertion of IGL enhancer (chr22) near the 3' of *CCND3* gene in case ID5. The breakpoints were detected by MP-WGS (cases ID3 and ID6), and whole-exome sequencing (case ID5), and further verified and refined to base pair resolution by Sanger sequencing in the 3 cases. There were 1, 2, and 3 base pair homology at the breakpoint junctions, respectively. (C) Verification of the cryptic IGK/*CCND3* insertion by FISH in case ID3 using the fusion probe IGK-enh (labeled in green) with *CCND3* (labeled in red). FISH analysis shows 2 red and 2 green signals in normal cells and the yellow arrows highlight cells with one red and one small green signal juxtaposed, indicating the presence of the IGK insertion. Magnifications of cells with the rearrangement were shown at the right side. (enh: enhancer). *Breakpoints estimated from MP-WGS data.

Figure 2. Conventional *CCND2* rearrangement in a cyclin D2⁺ MCL. (A) Circos plot with interchromosomal SVs detected by MP-WGS (black lines) and CNA detected by copy number arrays (blue for gains and red for losses) in case ID76. The conventional IGK/*CCND2* reciprocal translocation is indicated with two discontinuous lines for both derivative chromosomes. Among other SV, 12 clustered rearrangements were found between chromosomes 3 and 13 (at both regions of high copy gain). (B) A representative metaphase and the karyotype with the IGK/*CCND2* rearrangement (black discontinuous arrows) and other numerical and structural aberrations concordant with the results of MP-WGS and copy-number array: trisomy 7; loss of chromosome 9; and 2 marker chromosomes consistent with some of the rearranged chromosomes. (C) Schematic representation of the derivative chromosomes resulting from the translocation and zoomed image of *CCND2* locus. *All breakpoints were estimated from MP-WGS

analysis (chr2 in orange, containing the IGK enhancer and chr12 in blue containing *CCND2* gene).

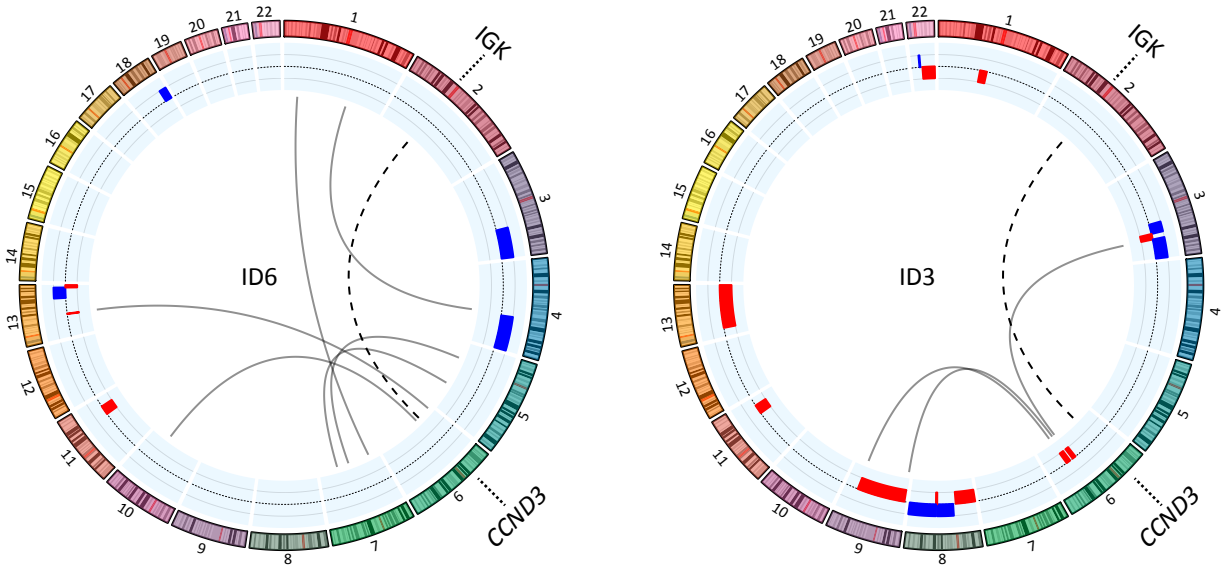
Figure 3. Expression of G1 phase cyclins by quantitative PCR. The expression of *CCND2*, *CCND3*, *CCNE1*, and *CCNE2* was represented according to 4 categories: MCL positive or negative for the *CCND2* break-apart FISH test (*CCND2* BAP+ and *CCND2* BAP-, respectively), chronic lymphocytic leukemia (CLL), and non-neoplastic lymphoid samples. Colored dots highlight cases with overexpression of *CCND2* (dark blue), *CCND3* (light blue), *CCNE1* and *CCNE2* (both in orange). The overexpression cut-off values were calculated as the mean plus 3 standard deviations in non-rearranged cases: 15.1 for *CCND2*, 6.2 for *CCND3*, 3 for *CCNE1*, and 2.4 for *CCNE2*.

Figure 4. Comprehensive genetic characterization of a MCL negative for *CCND1*, *CCND2*, and *CCND3* (ID73). (A) Tumor cells from the skin lesion had a blastoid morphology (Hematoxylin & Eosin; 40x), nuclear positivity for SOX11 (40x), and cyclin E1 (40x). (B) Circos plot representing from inner to outer circles: SVs detected by WGS (black lines for interchromosomal and red for intrachromosomal rearrangements) or detected only by MP-WGS (grey lines), CNA are represented in blue (gains and high copy gains) and red (losses and homozygous losses) palettes. In the outer circle the genes altered by mutations (green), genes disrupted by SVs (black), genes affected by homozygous deletions (red), and *CCNE2* gene with high-level gain (dark blue). No rearrangements of any cyclin or immunoglobulin genes could be detected. There were 2 dense clusters of interchromosomal rearrangements: i) one between chromosomes 3 and 6, at the regions of copy number loss; and ii) between chromosomes 8 and 18 at the regions of high copy gain. The gain of chromosome 19 and the loss of chromosome 22 were also supported as a reciprocal rearrangement by MP-WGS. (C) Chromosome 8 profile showing a partial 8q high-level gain (including the *CCNE2* gene locus, indicated by the red line) by two different techniques; SNP6.0 copy number arrays (top) and WGS analysis (bottom). (D) FISH with a locus specific *CCNE2* probe (green) and a centromeric chromosome 8 probe (orange) confirming that most tumors cells had at least 2 extra copies of *CCNE2* gene.

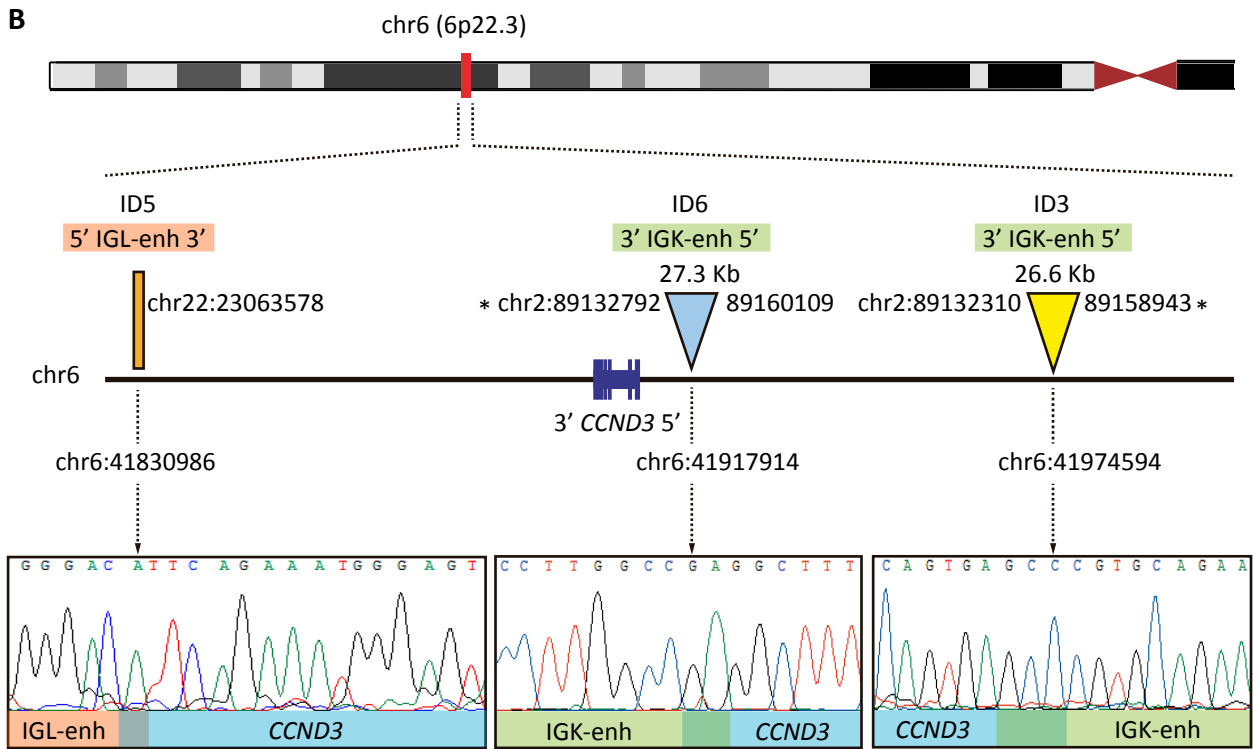
Figure 5. Global genetic landscape of the 56 cyclin D1⁺ MCL. Each MCL case is represented in a column and several specific molecular analysis in different rows. From top to bottom: 3 plots showing cyclin expression levels detected by qPCR (and by gene expression arrays in 3 cases, indicated with "X"); FISH results using break-apart or specific IGK-enh and *CCND2* or *CCND3* probes to detect cryptic rearrangements (rearranged cases in dark and light blue, respectively, and cryptic rearrangements are indicated with "C"); deletions of 9p21, 11q22, and 17p13 by copy number arrays (deletion in red, homozygous deletion in bordeaux); and presence of chromothripsis (green). The bar graph indicates the number of CNA detected in each case (NA, not available).

Figure 1

A



B



C

ID3 IGK-enh/CCND3

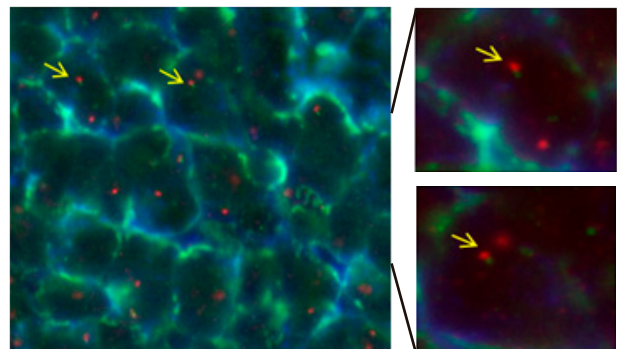


Figure 2

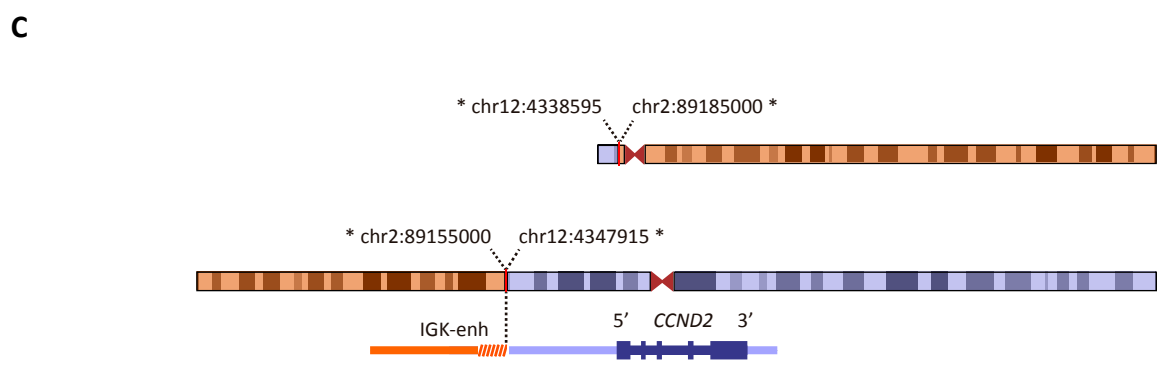
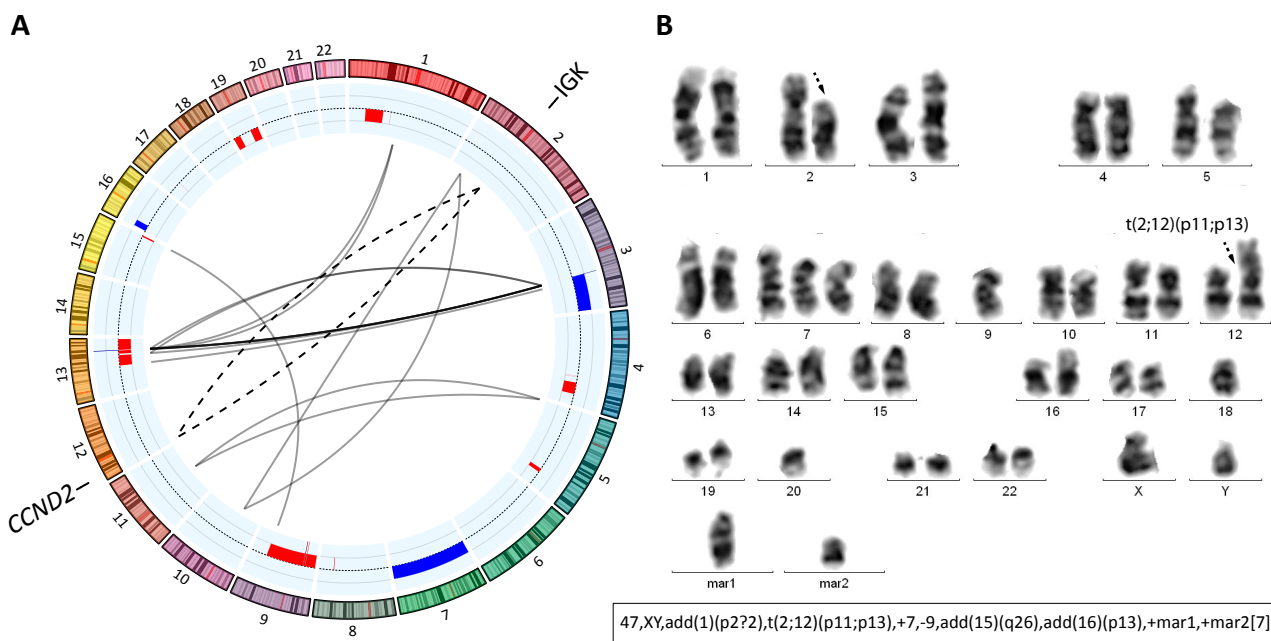


Figure 3

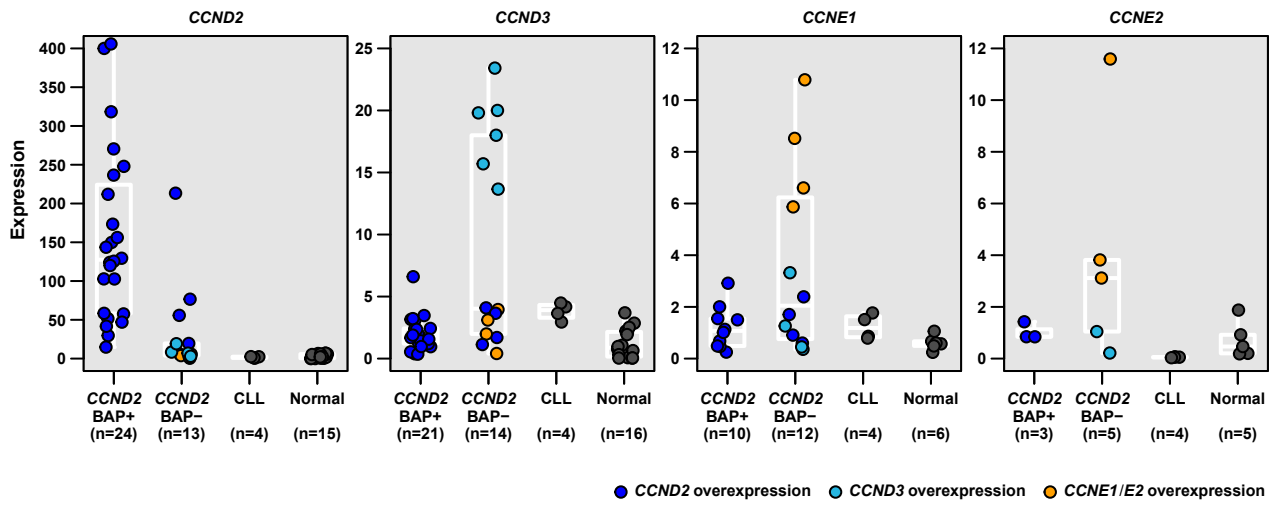
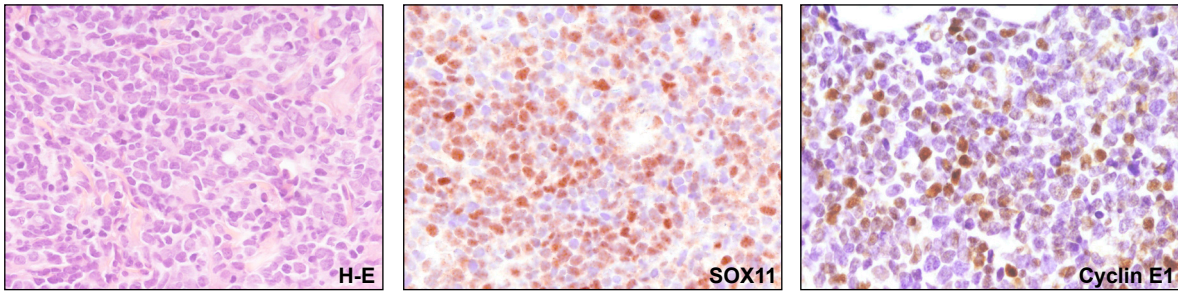
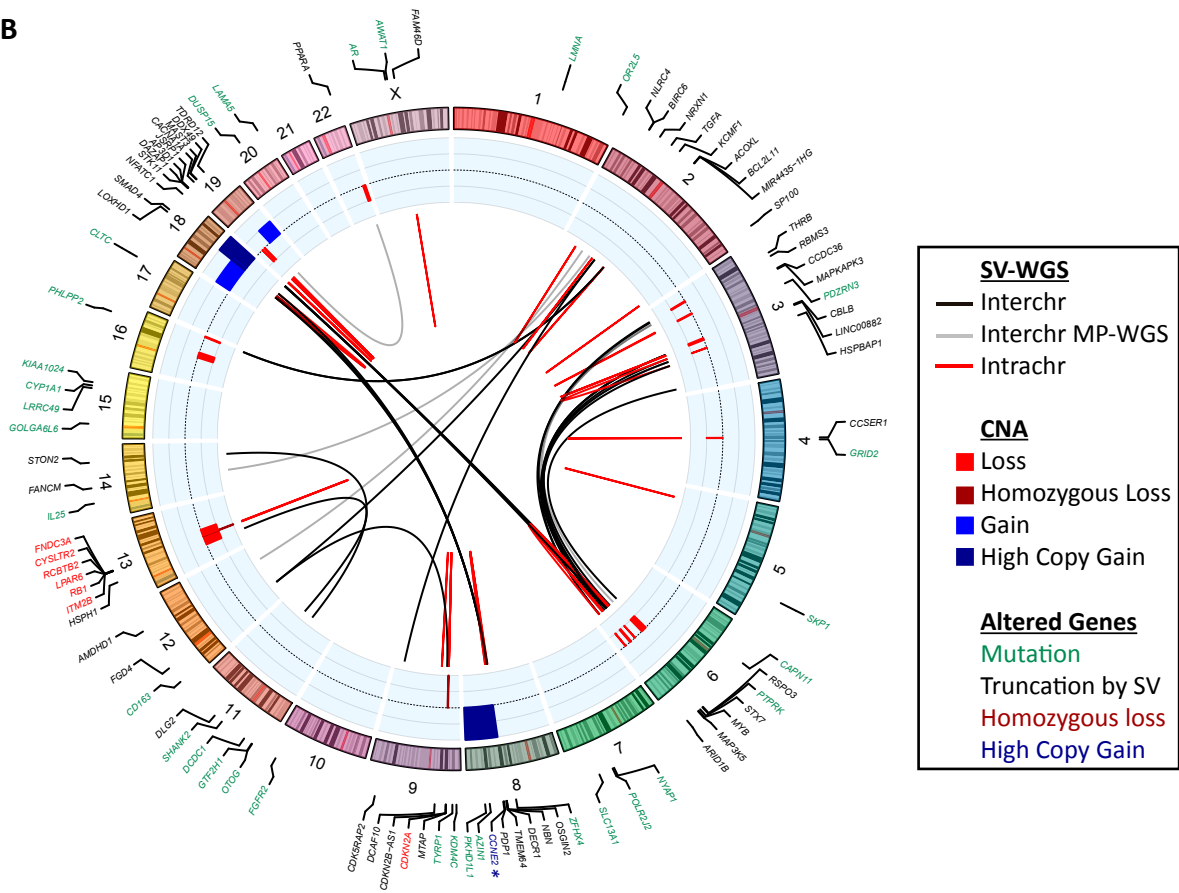


Figure 4

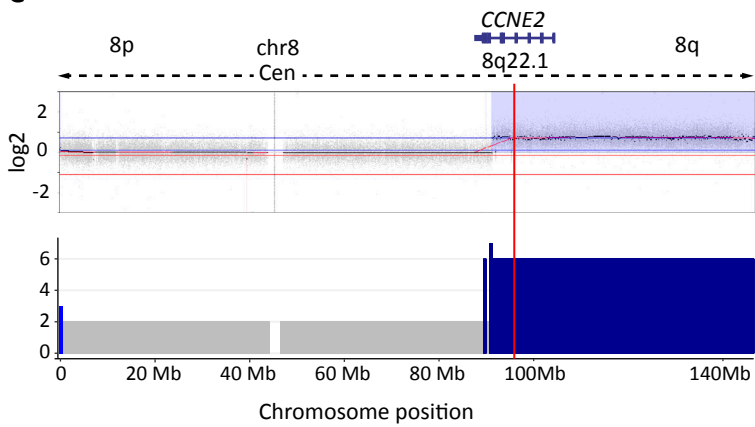
A



B



C



D

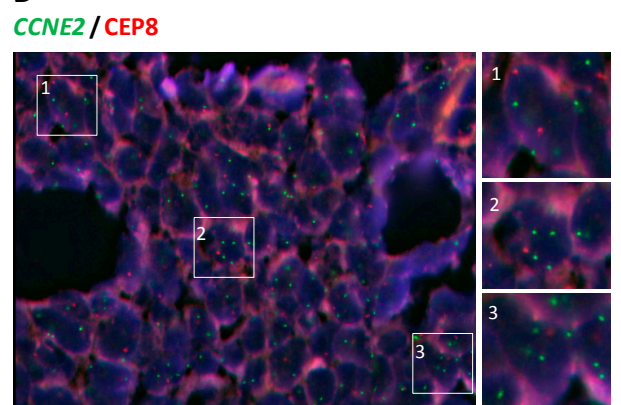


Figure 5

